Combination of natural silica and alumina sources for synthesis of MCM-22 zeolite

Worapak Tanwongwan [a], Nuwong Chollacoop [b], Kajornsak Faungnawakij [c], Suttichai Assabumrungrat [d], Puritut Nakhanivej [e], Apiluck Eiad-ua [a],[*]

[a] *College of Materials Innovation and Technology, King Mongkut's Institute of Technology Ladkrabang (KMITL), Chalongkrung Rd., Ladkrabang, Bangkok, 10520, Thailand*
[b] *National Energy Technology Center (ENTEC), National Science and Technology Development Agency (NSTDA), Phahonyothin Rd. Khlong Luang, Pathum Thani, 12120, Thailand*
[c] *National Nanotechnology Center (NANOTEC), National Science and Technology Development Agency (NSTDA), Phahonyothin Rd. Khlong Luang, Pathum Thani, 12120, Thailand*
[d] *Department of Chemical Engineering, Faculty of Engineering, Chulalongkorn University, Phayathai Rd., Phatumwan, Bangkok, 10330, Thailand*
[e] *Warwick Manufacturing Group (WMG), University of Warwick, Coventry, CV4 7AL, United Kingdom*

ARTICLE INFO

ABSTRACT

Zeolite has become a promising material that can potentially play a pivotal role in resolving environmental crises. Among zeolite families, MCM-22 zeolite shows outstanding intrinsic properties associated with the topology and porous structure, offering ion-exchange advantages for catalytic activity processes. The synthesis of MCM-22 zeolite becomes challenging when concerning the cost and catalytic performance. To overcome this bottleneck, we demonstrate a sustainable route of a hydrothermal process using natural resources as starting materials. Rice husk from agricultural waste was used as a silica source while natural clays (kaolin and bentonite) were applied as alumina sources. The products from natural sources were compared with the use of commercial starting materials, e.g., $NaAlO_2$ (for alumina) and Na_2SiO_3 and TEOS (for silica), in points of crystal, compositional, and morphological views. We showed that the high purity of MCM-22 zeolite can be obtained from rice husk silica (RHS) and aluminosilicate gel (ASG) extracted from kaolin, while the use of ASG extracted from bentonite tended to be unsuitable to generate the zeolite formation. We also studied the effects of reaction time and the ratio of RHS/ASG on the crystallinity and surface area of MCM-22. The architecture and acidity of an optimal product were explored by Nuclear magnetic resonance spectroscopy and Temperature-programmed desorption of ammonia, demonstrating the success of achieving well acidity.

1. Introduction

The critical increase of energy demand and environmental issues have underlined the importance of sustainable materials that can be potentially used in a wide range of applications regarding technical, industrial, agricultural, and ecological processes. Motivated by various candidates, zeolite has been highlighted as an outstanding porous material playing a crucial role in many industries. The beauty of physicochemical properties of zeolite offer a catalytic activity property for biomass conversion [1,2], wastewater treatment

---

[3–6], exhaust post-treatment [7], CO_2 capture [8–10], thermal energy storage [11], and production of H_2 [12,13]. Various types of zeolites present in nature as well as can be synthesized in laboratory. However, the MCM-22 zeolite (**M**obil **C**omposition of **M**atter No.22) first synthesized by Mobil researchers in 1990 [14] becomes the most suitable for the aforementioned applications and industries [15] as it offers the ion-exchange ability [16] owning to the MWW topology (**M**CM t**W**enty-t**W**o) [14,17] with two independent pore systems (e.g., a two-dimensional sinusoidal 10- membered ring (10-MR) with apertures 4 Å × 5.9 Å and a 12-membered ring (12-MR) large super cages with apertures 7.1 Å × 7.1 Å × 18.2 Å) [18,19]. Hence the main research stream on this material has been focusing on the sustainable synthetic routes to resolve the trade-off of cost and catalytic performance [20].

MCM-22 zeolite can be synthesized by a hydrothermal process using silica and alumina as starting materials and hexamethyleneimine (HMI) as a structure-directing agent providing two-dimensional (2D) structure. In particular, the calcination process can enhance the three-dimensional structure of MCM-22 zeolite as it aids in HMI removal [10,21,22]. The main issue of this route is the use of commercial silica and alumina as precursors [23]. Recently, natural source extraction was demonstrated as an alternative pathway for effectively receiving such starting materials. For instance, Rice Husk Silica (RHS) was extracted from rice husk waste from agriculture by acid treatment and calcination process to obtain pure silica [24,25]. Meanwhile, the natural clay including kaolin and bentonite can be used for the preparation of aluminosilicate gel (ASG) which is used as sustainable starting material for many types of zeolites such as zeolite A, X/Y, P, and ZSM-5 [26]. Nevertheless, the synthesis of MCM-22 type zeolite from kaolin and bentonite has yet to be exploited thus far.

Herein, we demonstrate the synthesis of MCM-22 zeolite through a combination of starting materials extracted from natural sources. Silica was extracted from rice husk by acid treatment and calcination process at various temperatures while alumina (in the form of ASG) was extracted from the natural clay including kaolin and bentonite. Both naturally extracted silica and alumina materials were used in the hydrothermal process to obtain MCM-22 zeolite. As for the baselines, the commercial sodium aluminate ($NaAlO_2$) was selected to combine with the RHS to compare with the use of ASG from natural clay. Also, the commercial sodium silicate (Na_2SiO_3) with tetraethyl orthosilicate (TEOS) were selected to combine with the ASG to compare with the use of RHS. The reaction time (3–7 days) and the ratios of RHS/ASG (9:1–3:1) were screened to optimize the final product. The overall experiments are shown in Scheme 1. The synthetic route established in this work can provide a big impact to wider environmental material community as well as be the design guideline for controlling and preparation of various types of zeolites.

2. Experimental

2.1. Extraction of silica from rice husk

The rice husk obtained from Nonthaburi, Thailand was washed by deionized (DI) water to remove impurities and dried at 100 °C for 12 h. After that, it was stirred in 3 M HCl solution at 100 °C for 2 h. Then, the product was filtered, washed, and neutralized by DI water and subsequently dried at 100 °C overnight. Finally, the treated rice husk was calcined at 700–1000 °C in muffle furnace for 12 h to obtain white RHS.
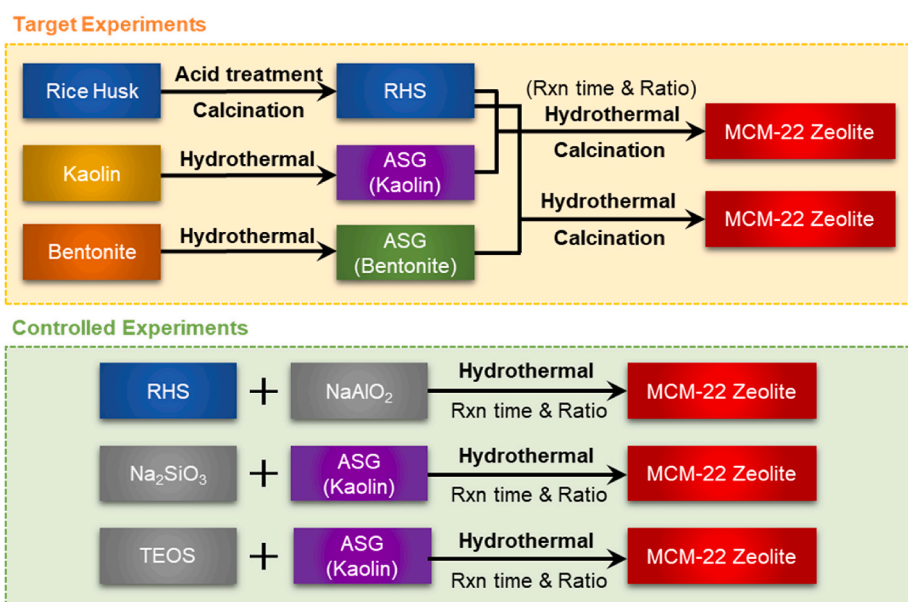
Scheme 1. | Schematic chart showing overall experiments for generating MCM-22 zeolites. RHS, ASG, and TEOS stand for Rice Husk Silica, Aluminosilicate Gel, and TetraEthyl OrthoSilicate, respectively.

2.2. Preparation of aluminosilicate gel (ASG) from natural clay

The elemental composition of natural clays including kaolin from Lampang province and bentonite from Lop Buri province in Thailand was analyzed by the EDX technique which elemental data was shown in Table S1. Clays were milled and a size that was lower than 90 μm was collected by mesh sieving to obtain the finest particle which was as fine as possible. Then, the hydrothermal process was performed at 200 °C for 8 h with 8 M of NaOH solution for the structure destruction. The reactor was quenched in ice after the process ended. When the system was cooled down, the solid phase was filtered, washed, and neutralized by DI water, and dried at 100 °C for 12 h and the basic liquid from the hydrothermal process was kept. Afterward, the solid powder was stirred in a 3 M HCl solution. Then, it was filtered, and the acid-liquid phase was collected. The acid liquid phase was adjusted to the pH of 7 b y a mother liquor from the hydrothermal process. The white aluminosilicate gel (ASG) was formed and dried in the oven. The EDX data demonstrate that the atomic ratio of Si/Al in ASG from kaolin and ASG from bentonite is 1.75 and 1.65, respectively.

2.3. Synthesis of MCM-22 zeolites

An alumina precursor was dissolved in NaOH solution (Carlo Erba) by stirring. Then, silica precursor was filled into the system followed by a structure-directing agent; hexamethylene imine (HMI) (Sigma-Aldrich) which was gradually dropped into the system for 30 min. The hydrothermal process was performed using a Teflon liner that was loaded into an autoclave reactor with a temperature controller, heating jacket, and stirring hotplate at 150 °C under a stirring state. Finally, the MCM-22(P) was filtered and washed with DI water, dried, and calcined at 540 °C for 20 h to obtain MCM-22 zeolites. The preliminary experiment is to explore the effect of starting materials, all commercial precursors were purchased from Sigma-Aldrich. An effect of alumina source was chosen as the first condition for this study. The commercial $NaAlO_2$ was selected to compare with the ASG from kaolin by the reaction condition based on Güray et al. [23] by default mol ratios were set as Si/Al = 30, Na/Si = 0.2, HMI/Si = 0.35, and H_2O/Si = 20, respectively. However, in the condition of using ASG from bentonite, the bentonite ASG was consumed into the reaction at the same amount as using ASG from kaolin in terms of weight to compare because both were the same achieved from natural clays. One ASG from different natural clays that shows a higher potential than another will be selected for the next experiment. The second condition is to study the effect of different Si sources by commercial Na_2SiO_3 and tetraethyl orthosilicate (TEOS) were selected for the comparison. All silica content from different sources in this condition was calculated to equal by mol. Finally, the best condition obtained from natural sources was taken to study in the next conditions consisting of an effect of reaction time (3–7 days) and an effect of weight ratio of RHS/ASG (9:1–3:1).

2.4. Characterization

The purity of RHS was confirmed by a Raman spectrometer (DXR SmartRaman, Thermo Scientific). The crystallography of materials was analyzed by X-ray diffraction (XRD) technique (SmartLab, Rigaku). The surface area and porosity of materials were studied by N_2 adsorption-desorption analysis technique (autosorb iQ, Quantachrome instruments) where the samples were degassed at 300 °C for 6 h with a heating rate of 10 °C min^{-1} before measurement. The structure and functional groups of materials were carried out by Fourier-transform infrared (FT-IR) spectroscopy (Spectrum Two, PerkinElmer). The thermal stability of materials was evaluated by Thermogravimetric analyzer (TG 209 F^3 Tarsus, NETZSCH) under the N_2 atmosphere. The morphology and composition of materials were observed by scanning electron microscopy (SEM) with the energy dispersive X-ray (EDX) spectroscopy (EVO MA10, Zeiss). The chemical identity of the samples was investigated by solid-state Nuclear magnetic resonance (NMR) spectroscopy (JNM-ECZ-400 R/S1, JEOL) at 400 MHz. The acidity was studied by NH_3-TPD analysis (Belcat B, BEL JAPAN, Inc.) where the process for ammonium desorption analysis was carried out according to the literature [27].
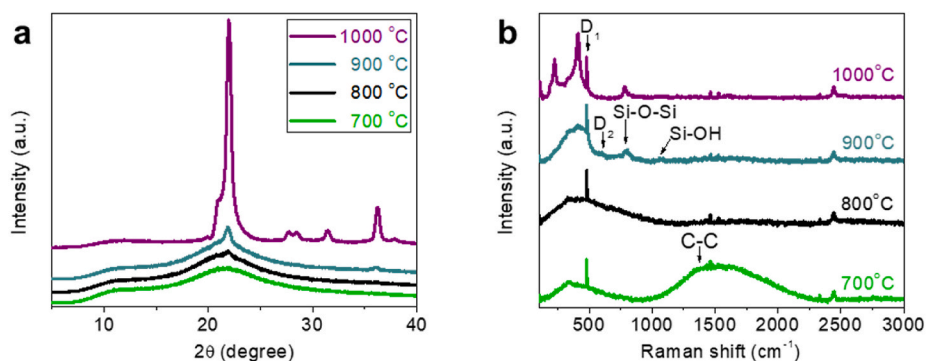

Fig. 1. | Extraction of Silica from Rice Husk. (a) X-ray diffractograms and **(b)** Raman spectra of Rice Husk Silica at the various calcination temperatures.

3. Result and discussion

3.1. Extraction of silica from rice husk

The treated rice husk was calcined at the temperature of 700–1000 °C for 12 h to obtain RHS. As shown in XRD patterns in Fig. 1a, the amorphous silica is the major component of RHS calcined at 700–800 °C while the crystalline silica appears at the calcination temperature above 900 °C. Such silica crystals become more pronounced at the calcination temperature of 1000 °C. We further investigated the purity of each sample using Raman spectroscopy as presented in Fig. 1b. With the low calcination temperature of 700 °C, the RHS samples were contaminated by the carbon in the structure as the peak of *C*–C vibration appears at 1378 cm^{-1} [28]. The *C*–C vibration peak is decreased with the increase of calcination temperature and is completely diminished at the temperature above 800 °C. The silica peak at the 483 cm^{-1} is identified as *Si–O*–Si bending modes of the 4-membered rings (D_1). At 900 °C, the peak of 3-membered rings (D_2) from the condensation of -SiOH groups appears at 588 cm^{-1} due to the increasing of D_1 intensity, and the symmetric stretching of *Si–O*–Si and Si–OH are located at 795 cm^{-1}, and 985 cm^{-1}, respectively [29]. The intensity of D_1 is increased following the increase of calcination temperature while the D_2 (associated with -SiOH) and the *Si–O*–H stretching are decreased and finally disappeared at 1000 °C indicating that the OH bond is completely eliminated.

3.2. Crystallization of MCM-22 zeolites

All MCM-22 zeolites were synthesized by hydrothermal process at 150 °C in which the XRD pattern of each sample is presented in Fig. 2. Various alumina sources including commercial NaAlO$_2$, ASG from kaolin, and ASG from bentonite influence the crystalline structure of MCM-22 zeolites (Fig. 2a). Although the MCM-22 zeolites generated from all alumina sources shows similar crystal lattice (i.e., similar XRD patterns) [30], the commercial NaAlO$_2$ is suggested to be the most effective source for this process following by ASG from kaolin. Meanwhile, the ASG from bentonite shows the lowest ability to crystalize MCM-22 as broadened XRD pattern is observed. This can be confirmed by the crystallinity of 57% for the MCM-22 from commercial NaAlO$_2$ which is higher than those of 39% and 16% for MCM-22 from kaolin ASG and bentonite ASG, respectively. This phenomenon is supported by the EDX results in Table S2. MCM-22 using NaAlO$_2$ as an Al source has the lowest Si/Al ratio compared to MCM-22 using of ASG from kaolin and ASG from bentonite. An outstanding higher ratio of Si/Al on the products using ASG from kaolin was mean a lower amount of aluminum content and affected
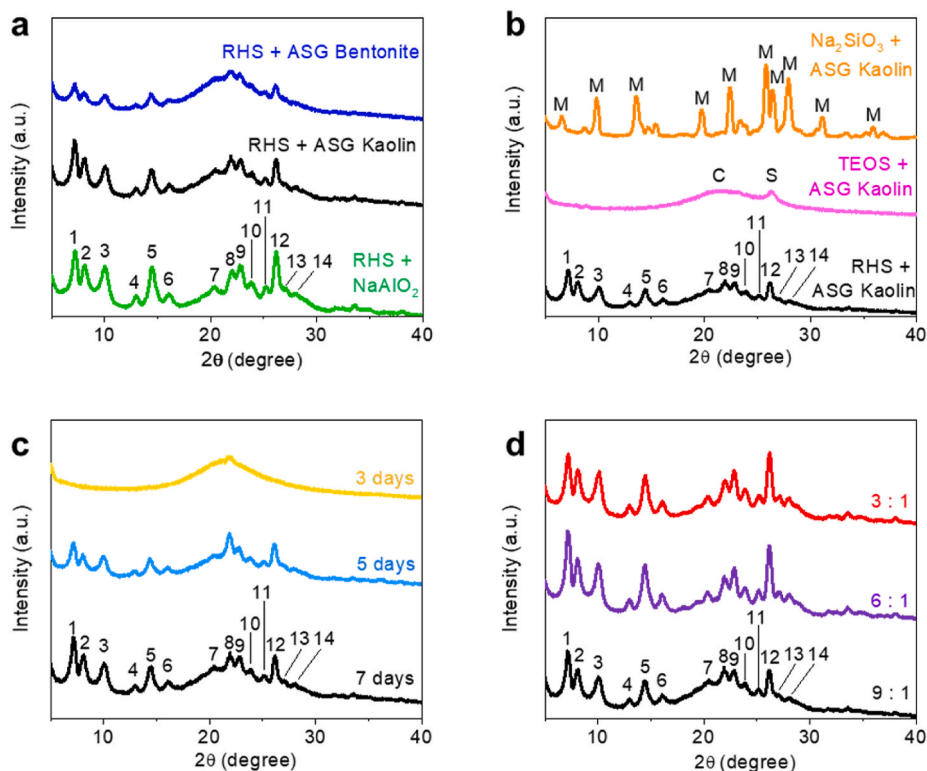

Fig. 2. | Crystallization of MCM-22 Zeolites. X-ray diffractograms of final products with different synthesized conditions by **(a)** effect of Al sources, **(b)** effect of Si sources (where M, C, and S stand for mordenite, carbon, and silica, respectively), **(c)** effect of reaction time, and **(d)** effect of RHS/ASG ratios. Peaks 1–14 correspond to lattice planes of (100), (101), (102), (111), (201), (202), (212), (301), (302), (214), (220), (310), (312), and (117), respectively.

the lower crystal formation of zeolite. Using ASG from bentonite as an Al source resulted in the lowest crystalline formation which was corresponding to the highest Si/Al ratio. That might be because of the adulterating of impurities ions in bentonite clay (see Table S1) that were leached in the step of Si and Al extraction by acid. It affects the lower total content of Al and Si in ASG from bentonite, although the ratio was similar to Si/Al ratios in the kaolin ASG. This means that in the same amount, the ASG from bentonite had a significantly lower potential for use as starting material of MCM-22 than ASG from kaolin. So, the ASG from kaolin was selected to use as an Al source for study in further conditions.

The condition of various Si sources led to astounding results. As shown in Fig. 2b, clear peaks of MCM-22 zeolite only appear in the case of using RHS as a silica source. The use of TEOS is unable to generate the structure of MCM-22 zeolite as only carbon and SiO_2 peaks are dominant. This is probably due to the interaction between TEOS and the HMI in the reaction leading to a solid white gel formation that interrupts the mixing of starting materials. This leaves lot of TEOS inactive and there is only a separate group of TEOS and ASG in the system. After the calcination process, TEOS was decomposed into a silicon-coated carbon sphere [31]. Using Na_2SiO_3 as a Si source generates the Mordenite zeolite (MOR) with 58% of crystallinity while MCM-22 zeolite is completely absent. This is due to the Na_2SiO_3 is Na_2O rich which is appropriate for the formation of MOR-type zeolite [23]. Therefore, further conditions to be studied hereafter are performed using ASG from kaolin as the alumina source while RHS was used as a source of silica for the synthesis of MCM-22 zeolite in this article.

An effect of reaction time on the crystal structure of zeolite is shown in Fig. 2c. After 3 days, the structure of MCM-22 zeolite is not generated as the structure of sample is mainly amorphous silica. The longer reaction time leads to the formation of zeolite, i.e., the MCM-22 structure is clearly observed with 34% crystallinity after 5 days of reaction. In particular, the reaction time of 7 days even enhance the crystallinity up to 39%. It is noteworthy that although the clear formation of MCM-22 is observed for the 5 day reaction, the peak intensities of lattice planes (100) and (310) (associated with the intra-layer of zeolite [32]) are lower than that of the one using 7 day reaction. This observation was indicated that the intra-structure of MCM-22 is yet to completely formed after 5 days of reaction.

Fig. 2d exhibits the effect of RHS/ASG ratios on the structure formation of MCM-22 zeolite. At the ratio of 9:1, the relative crystallinity is estimated as 39%. Such value increases to 66% for the ratio of 6:1 and all peak intensities are increased especially for the lattice planes of (312) and (117). However, the crystallinity tends to gradually decrease with the relative crystallinity of 63% for the lower ratio of 3:1. Specifically, a significant change is observed at the lattice planes (100) and (310). The ratio of these planes' intensity decreases with the decreasing of RHS/ASG ratio; however, this intensity ratio slightly decreases for the RHS/ASG ratio of 6:1 compared to the condition of 9:1. The obvious change is observed for the condition of 3:1 RHS/ASG where the intensity of (100) plane is decreased and lower than an intensity of (310) plane. The phenomenon suggests that a low Si content leads to the decreasing of zeolite
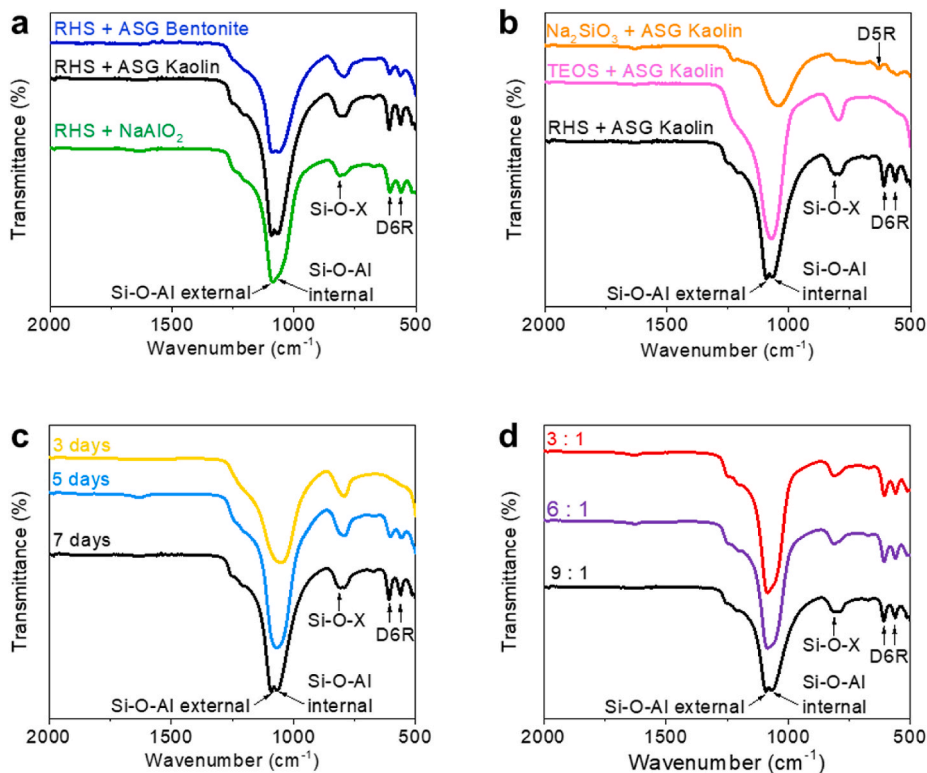

Fig. 3. | Chemical Structure of MCM-22 Zeolites. FT-IR spectra of final products with different synthesized conditions by **(a)** effect of Al sources, **(b)** effect of Si sources, **(c)** effect of reaction time, and **(d)** effect of RHS/ASG ratios.

fragment formation on (100) lattice plane [32].

3.3. Chemical structure of MCM-22 zeolites

To gain more insight in how starting materials control the chemical structure of MCM-22 zeolite, we investigated the IR characteristic of each sample as presented in Fig. 3. The MWW structure of MCM-22 zeolite is confirmed by unique characteristic vibration of the secondary building block of double 6- membered rings (D6R) at a wavenumber of 567 and 614 cm^{-1}. Symmetric stretching of Si–O-X (where X = Si or Al) shows at 813 cm^{-1}. In particular, the internal and external asymmetric vibrations of Si–O–Al locate at 1084 cm^{-1} and 1098 cm^{-1}, respectively [18,19,33]. The identity of these Si–O–Al vibrations are dependent on the Al sources. As shown in Fig. 3a, the use of NaAlO$_2$ leads to the stronger external vibration peak than the internal one, consistent with the XRD result that the use of NaAlO$_2$ leads to the high crystal structure growth. In the condition of using ASG from kaolin, the external and internal vibration peaks are clearly separated and broadened, suggesting the lower crystal growth of MCM-22. The use of ASG from bentonite also enhances the separation of asymmetric Si–O–Al vibrations, yet the peaks are broadened and still merged, indicating the lowest structure formation ability of MCM-22 zeolite.

For the use of various Si sources, it is clearly observed that the TEOS is unable to generate MCM-22 zeolite formation as the unique D6R vibration is absent (Fig. 3b) [34]. Meanwhile, the IR spectrum of using Na$_2$SiO$_3$ confirms a structure of MOR-type zeolite as the band of double 5-membered rings (D5R) presented at a wavenumber of 633 cm^{-1}. In addition, a small peak at a wavenumber of 800 cm^{-1} is from the symmetric stretching modes of O-X-O and the main peak at a wavenumber of 1046 cm^{-1} belongs to asymmetric stretching of O–Si–O [35].

The chemical structure of MCM-22 zeolites is dependent on reaction time as well. Fig. 3c shows that the D6R vibrations are absent and only symmetric stretching peaks of Si–O-X and internal asymmetric vibration peaks of Si–O–Al are present for the 3-day reaction conditions, indicating unsuccessful MCM-22 crystal growth. After 5 days of reaction, the D6R peaks are observed with low intensity, and only the internal asymmetric vibrations of Si–O–Al are presented. For the 7-day reaction time, the MCM-22 zeolite displays the complete formation of functional groups, with sharp peak intensities. The internal and external vibration peaks of Si–O–Al are clearly
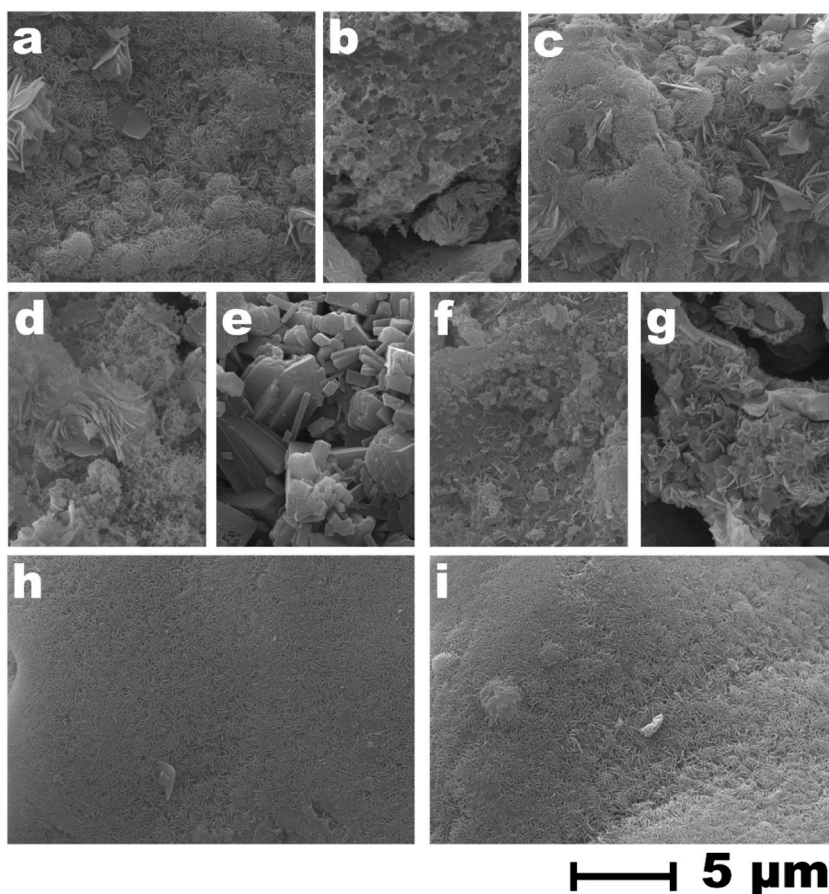

Fig. 4. | **Morphology of MCM-22 Zeolites.** SEM images at 20,000× magnifications of final products with different synthesized conditions by **(a)** RHS + NaAlO$_2$, **(b)** RHS + ASG from Bentonite, **(c)** RHS + ASG from Kaolin, **(d)** TEOS + ASG from Kaolin, **(e)** Na$_2$SiO$_3$ + ASG from Kaolin, **(f)** 3 days, **(g)** 5 days, **(h)** RHS/ASG = 6:1, and **(i)** RHS/ASG = 3:1. Scale bars, 5 μm.
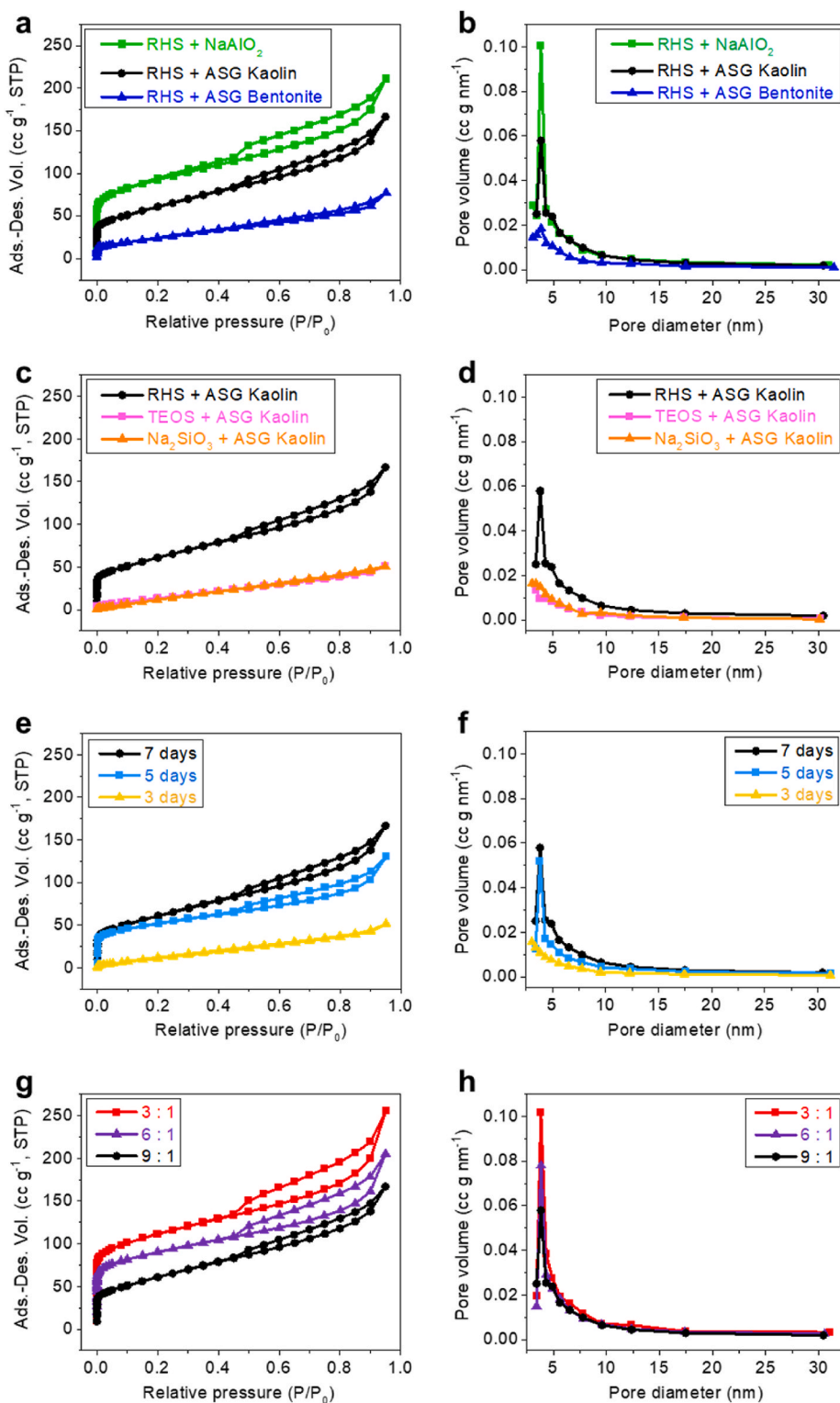
Fig. 5. | Surface Area and Porous Properties of MCM-22 Zeolites. N$_2$ adsorption-desorption isotherm and Barrett-Joyner-Halenda (BJH) pore size distribution of final products with different synthesized conditions by **(a–b)** effect of Al sources, **(c–d)** effect of Si sources, **(e–f)** effect of reaction time, and **(g–h)** effect of RHS/ASG ratios.

separated, suggesting sufficient reaction time to growth MCM-22.

The effect of the Si/Al ratio is one of the significant factors affecting the functional group of MCM-22 zeolites. As shown in Fig. 3d, the ratio of RHH/ASG at 9:1 leads to the lowest intensity ratio of *Si*–*O*–Al vibration peaks. Moreover, the peak of external and internal vibrations was clearly separated with the similar intensity. For the condition of 6:1 and 3:1 RHS/ASG ratio, the internal and external vibration peaks are merged and broadened. Particularly, the peak intensity of external vibration is more dominant to the internal vibration peak, indicating that the formation of zeolite's intra-layer is minor owning to the lowest amount of Si content, in line with the XRD results.

3.4. Morphology observation of MCM-22

The morphology of all products was monitored using SEM with the magnification of 20,000× as shown in Fig. 4. The use of NaAlO$_2$ results in the fine formation of MCM-22 zeolite (Fig. 4a) which has a straw ball-like shape with a size approximately 2 μm, containing many petals with a thickness lower than 100 nm in each ball. The residual Si sheets are still presented with the size for about 3–4 μm. Using ASG from bentonite as an Al precursor shows rather poor results (Fig. 4b). The straw ball-like MCM-22 clusters are rarely presented and the pieces of zeolite petals grow a little on the surface of Si bulks providing the shape like a sponge. The morphology of MCM-22 using ASG from kaolin as Al sources shows a similar character to the MCM-22 from NaAlO$_2$, yet the number of residual Si sheets is higher (Fig. 4c). Meanwhile, using TEOS as a Si source shows the completely absent of MCM-22 zeolite. As shown in Fig. 4d, the surface morphology of materials shows a large Si sheets and carbon particles which coated by fluffy Si flakes. Fig. 4e demonstrated that the use of Na$_2$SiO$_3$ as a Si source resulted in high purity of MOR-type zeolite which shows all over of plate-liked and prismatic particles [35]. The size of MOR-zeolite particles was founded in the range of about 1–5 μm.

The effect of reaction times leads to various behavior of MCM-22 zeolite formation. On 3 days of reaction time (Fig. 4f), the sample shows the absences of the MCM-22 straw ball-liked cluster. However, the surface of the Si bulk shows the initial stage of zeolite's petals formation. Fig. 4g shows the morphology of MCM-22 zeolite synthesized with 5 days of reaction time, the zeolite petals were formed and tended to aggregate, separating from the surface of amorphous Si for the formation of MCM-22 straw ball-liked. However, the petals of zeolite in this condition are rather huge in size and many petals showed the shape of rough flake liked which have a diameter of about 1–2 μm. Furthermore, the gigantic plates of amorphous Si reside on Si sheets, confirming the low crystallization of zeolite from the low reaction times.

The morphologies of MCM-22 zeolites which were synthesized using the ratios of RHS/ASG of 6:1 and 3:1 are shown in Fig. 4h and i. Both conditions provide similar morphological results. The zeolite petals are gathered like a vast field. The petals are tightly and densely agglomerated which shows excellent zeolite structure formation. The thickness of petals was lower than 100 nm and the residual amorphous Si sheets were observed in a low amount. The morphology of these two outstanding products at the zoomed out of magnification at 5,000× can be observed that the field of zeolite petals was clustered as large particles, these large particle shapes seemed to be like spherical/plates or shuttles with the size of about 45 μm. The SEM image at the magnification of 5,000× of MCM-22 zeolite synthesized on the ratios of RHS/ASG of 6:1 and 3:1 are shown in Fig. S1a-b, respectively. Compared with the use of 9:1 RHS/ASG ratio shown in Fig. 4c, the reduction of the RHS/ASG ratio tends to result in a better formation of the MCM-22 structure. All evolutions and developments of MCM-22 zeolite surface morphology are according to all results from previous characteristic techniques.

3.5. Surface area and porous structure

We further investigated the effect of starting materials on surface area and porous properties of MCM-22 zeolites through N$_2$ adsorption-desorption isotherm as shown in Fig. 5. The uses of NaAlO$_2$ and ASG from kaolin as alumina sources result in MCM-22 showing Type IV with H4 hysteresis loop which indicates the mesopores and micropores [36]. NaAlO$_2$ provides the highest adsorption-desorption behavior of MCM-22 among the Al sources as shown in Fig. 5a. The pore size distribution curves of MCM-22 zeolites derived from all alumina sources in Fig. 5b display the highest pore size centering at 3.8 nm within the distribution range of 3–31 nm. NaAlO$_2$-MCM-22 shows highest 3.8-nm pore volume among other Al sources. This results in NaAlO$_2$-MCM-22 has the surface area of 328 m^2 g^{-1} which is higher than Nat-MCM-22 from kaolin ASG (219 m^2 g^{-1}) and bentonite ASG (90 m^2 g^{-1}). The larger surface area of NaAlO$_2$-MCM-22 is in line with the observation of highest micropore distribution.

The surface and porous properties of zeolite products are also significantly dependent on sources of Si. The use of RHS as a Si source generated the structure of MCM-22 containing mesoporous and microporous. Nevertheless, the use of TEOS and Na$_2$SiO$_3$ gave a completely different result. As presented in Fig. 5c, using TEOS results in forming a silicon-coated carbon sphere. N$_2$ adsorption-desorption isotherm of this product shows the IV types, however, the hysteresis loop is very narrow, and an adsorption-desorption volume was very low by maximum volume is about 50 cc g^{-1}, STP. The MOR-type zeolite synthesized by using Na$_2$SiO$_3$ as a Si source shows the same hysteresis loop shapes and similar adsorption-desorption volume as the use of TEOS. Fig. 5d shows the pore size distribution of zeolites that were derived from different Si sources. All products have a similar range of pore size distribution of about 3 nm–30 nm. However, the pore volume of products synthesized from TEOS and Na$_2$SiO$_3$ was way lower than using RHS. The highest pore size distribution of MCM-22 zeolite is centered at 3.8 nm while the highest pore size distribution of a silicon-coated carbon sphere and MOR-type zeolite locate at 3.4 and 3.1 nm, respectively. In addition, the surface area and porous properties confirm that the using of TEOS and Na$_2$SiO$_3$ generates only mesoporous with the approximated surface area of 58 and 77 m^2 g^{-1}, respectively.

The effect of reaction time on surface area and porosity of MCM-22 zeolites are further discussed (Fig. 5e). All as-synthesized zeolites from various reaction times show IV-type isotherms. However, an adsorption-desorption volume is enhanced with the

increasing reaction time. At the condition of 3 days, the hysteresis loop is narrowest and shows the lowest adsorption-desorption volume. The hysteresis loop is wider on the condition of 5 days and the highest adsorption-desorption volume is reached for the condition of 7 days of crystallization. Fig. 5f shows the pore size distribution of zeolite at different reaction times ranging from 3 to 31 nm. The pore volume of zeolite on 3 days of reaction is the lowest. The highest pore size distribution of products synthesized in 3 days is centered at 3 nm while this value shifts to 3.8 nm when the reactions are extended to 5 and 7 days. Furthermore, reaction with 3-day time provides the lowest surface area with only mesoporous, while the reaction for 7 days enhances the surface area and mesoporous structure (see Table 1).

For the influence of RHS/ASG ratio, the adsorption-desorption volume is increased with the decreasing of RHS/ASG ratio as shown in Fig. 5g. The similar trend goes to the width of hysteresis loops as well. The pore size distribution of all products is in the range of 3–31 nm (Fig. 5h), in line with other condition studies. The pore volume is enhanced by the decreasing of RHS/ASG ratio, and the highest pore size distribution is centered at 3.8 nm for all MCM-22 zeolites. Data in Table 1 confirms that the area and volume of micropores are in accordance with the total surface area, but the difference is presented in a term of mesoporous. This phenomenon can be related to the EDX result. The condition of RHS/ASG as 9:1 provides the low amount of Al content which affects the formation of zeolite structure. The crystallization of zeolite in this condition is low and mostly generates mesoporous. The lower amount of Si content in the condition of RHS/ASG as 6:1 shows more advantage, i.e., the role of Al for zeolite structure formation is dominant when decreasing the RHS/ASG ratio and it enhances the structure formation of zeolite, resulting in the decrease of mesoporous area while the microporous area is obtained significantly. Remarkably, a reduction of the RHS/ASG ratio to 3:1 in turn enhances mesoporous area. This is owning to the low Si content affects more creation of mesoporous and removal of zeolite crystallite in the intra-layer [32], leading to the ever-increasing mesopore and the slight decrease of relative crystallinity, consistent with XRD and FT-IR results.

3.6. Thermal stability analysis

The TG curve of MCM-22 was presented in Fig. 6. All products synthesized using different Al sources show the most weight loss within the range of 30–150 °C as shown in Fig. 6a which corresponds to the loss of water molecules physisorbed in the pores or cavities. The use of $NaAlO_2$ as an alumina precursor displays the biggest weight loss of about 7% followed by using ASG from kaolin (about 3%) and ASG from bentonite (about 2%), respectively. This result was in accordance with the surface area and porous property analyses, i. e., the use of $NaAlO_2$ leads to the highest surface area and biggest pore volume – hence the high amount of water adsorbed and subsequently the most weight loss when running TGA – while the use of ASG from bentonite leads to the lowest surface area, thereby showing opposite result regarding the weight loss.

The TG curve of final materials synthesized using various Si sources are presented in Fig. 6b. Using RHS affects to the surface properties of zeolite as well. The huge weight loss at 30–150 °C is due to the desorption of water molecules in cavities. In the condition of using TEOS, the curve is very downward in the early stages ranging from 30 to 250 °C which indicates a wasting of water molecules and a degradation of organic material (carbon) in the structure [37] which reducing the weight of the product by about 5–6%. Afterward, a slight weight decreases points to the structural stability of the SiO_2 bulk [38]. Using Na_2SiO_3 as a Si precursor shows the largest amount of weight loss for approximately 12% ranging from 30 to 350 °C due to the releasing of water adsorbed and the dehydration of Na^+ ions in MOR-type zeolite's channels [35].

A reaction time insignificantly affects the thermal stability of products. As represented in Fig. 6c, the amount of weight loss is enhanced with the increasing of reaction time. This phenomenon corresponds to the surface and porous properties, i.e., the smallest weight loss is observed in the condition of the shortest reaction time because of the lowest surface area and pore volume. In contrast, the longest crystallization time generates the highest surface potential which results in the highest weight loss due to a large amount of water adsorbed. However, the mass losses are not much different which was about 1–3%.

For the effect of RHS/ASG ratios, the most weight loss of all samples was observed in the same range of 30–150 °C as shown in Fig. 6d where the lowest RHS/ASG ratio affects the largest amount of weight reduction, approximately 8%. Meanwhile, the higher RHS/ASG ratios of 6:1 and 9:1 result in lower weight losses of 6% and 2%, respectively. The fundamental behind this phenomenon is according to an increase of surface area by reducing the RHS/ASG ratio which enhances a humidity adsorption.

Table 1

Surface areas and pore properties of Si–Al based materials with different synthesized conditions.

Conditions	Surface area (m^2/g)	Micropore volume (cc/g)	Micropore area (m^2/g)	Mesopore area (m^2/g)	Average pore diameter (nm)
[a]**RHS + ASG Bentonite**	90.251	N/A	N/A	90.251	5.3
[a]**RHS + ASG Kaolin**	218.504	0.002	7.502	211.002	4.72
RHS + NaAlO$_2$	328.468	0.051	117.444	211.024	3.98
TEOS + ASG Kaolin	58.013	0	0	58.013	5.4
Na$_2$SiO$_3$ + ASG Kaolin	77.469	0	0	77.469	4.05
[b]**3 days**	55.308	0	0	55.308	5.77
[b]**5 days**	183.079	0.024	55.637	127.442	4.4
[c]**6:1**	323.973	0.064	150.498	173.475	3.92
[c]**3:1**	399.467	0.079	187.463	212.004	3.96

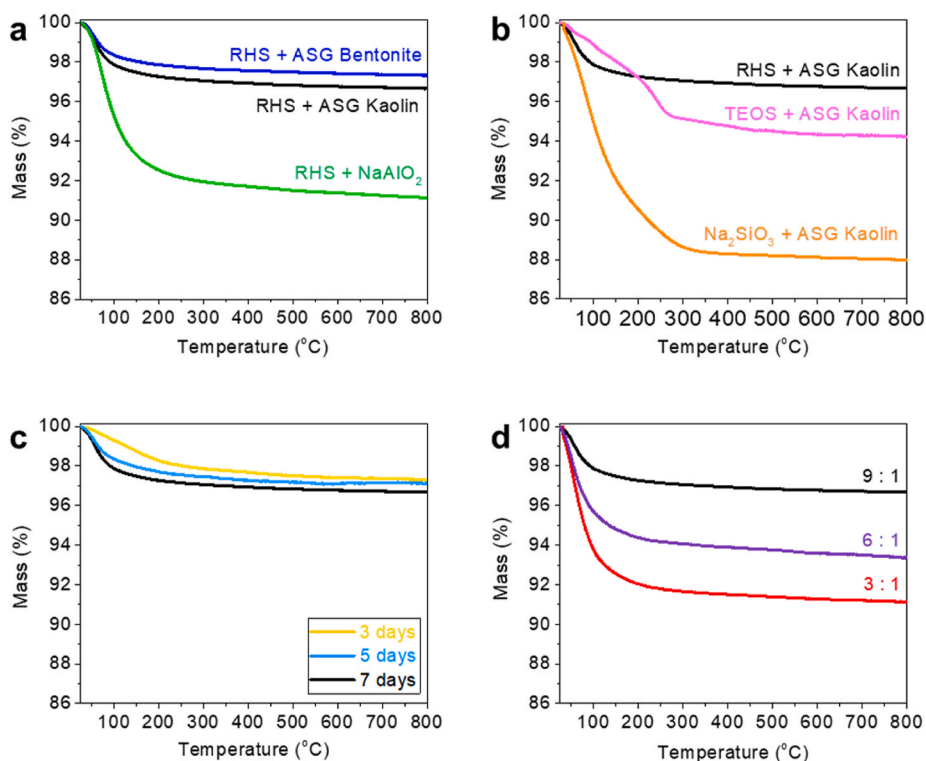[a] RHS/ASG = 9:1, 7 days.
[b] RHS/ASG = 9:1.
[c] 7 days.

Fig. 6. | **Thermal Stability of MCM-22 Zeolites.** Thermogravimetric Analysis curves of final products with different synthesized conditions by **(a)** effect of Al sources, **(b)** effect of Si sources, **(c)** effect of reaction time, and **(d)** effect of RHS/ASG ratios.

3.7. Acidity analysis

MCM-22 zeolite synthesized by using RHS and ASG from kaolin for 7 days with the RHS/ASG ratio of 3:1 was selected to be an optimized condition, thereby being able to provide insight about chemical architecture and structure. ^{27}Al MAS-NMR spectrum of this product is shown in Fig. 7a by all states related to the literature [39] with about +7 shifted. A low-frequency sharp signal at ~5 ppm refers to extra-framework octahedral aluminum in structure [40] and a broad peak at ~55 ppm is identified as aluminum on an external surface and/or in a large lattice's cavity [41]. The last peak at 61–63 ppm is identified as tetrahedral aluminum postured in micropore.

Fig. 7b presents the ^{1}H MAS-NMR spectrum of this sample by about +1 shifted from the literature. Signals at the low frequency indicated weak acidic terminal SiOH groups which were generated in crystal defects and on external surfaces of zeolite structures (likewise the extra-framework AlOH groups). A low peak intensity at ~3 ppm associates with the terminal OH bond of silanol groups on zeolite's external surface. The low signal of this peak is due to the low ratio of RHS/ASG. A broad signal at ~4 ppm originates as hydroxyl groups on aluminum extra-framework, this peak has a higher intensity than the peak of silanol groups because of the low amount of RHS/ASG ratio enhances the aluminum species creation. The high acidity of this sample is confirmed by the high peak intensity of acidic OH groups of Si(OH)Al residing at ~6.5 ppm [39,41,42]. Furthermore, the peak shoulder at ~4.5 ppm indicates a high number of protons of Brønsted acid sites in this sample. Such Brønsted acid sites are the results of interaction between aluminum and silanol groups where the RHS/ASG ratio is low.

^{29}Si MAS-NMR analysis can support the aforementioned discussion, revealing the hexagonal structure in the *b*-axis as shown in Fig. 7c. Based on the assumption that MWW-type zeolite is a hexagonal structure, each cell will consist of eight T positions that have nonequivalent crystallography. An Al^{3+} ion is possible to dominate the center position and generate a balance anion by a cation of alkaline earth metal or hydrogen ion [43]. Fig. 7d presents ^{29}Si MAS-NMR deconvoluted spectra of MCM-22 zeolite. Intensities of the T_{3+4+5}, T_8, and T_7 peaks are higher than that of T_2 peak, consistent with the literature [39]. Especially, peaks of the T_3, T_4, and T_5 positions are fused together into single peak. Moreover, the peak intensities of the T_7 and T_8 positions are lower than those of T_{3+4+5} peak as well. Such phenomena are because of the low Si content in the zeolite structure resulting in the minor defects with a low signal of the T_2 site. Furthermore, it is possible that aluminum atoms can play significant role by residing at the 12-MR super cages and 2D sinusoidal 10-MR to interact with silica species, giving the notable high intensity of T_{3+4+5} peak.

An acidity of MCM-22 zeolite synthesized by using RHS and ASG from kaolin at 7 days with the RHS/ASG ratio of 3:1 was further confirmed by the NH$_3$-TPD analysis technique. A TPD profile presented in Fig. 7e suggests that this zeolite sample contains 2-types of acidities. The deconvoluted peak indicates a weak acidity desorption curve centered at 220 °C with an acidity of 0.42 mmol NH$_3$ g^{-1} while a desorption curve of medium acidity is centered at 330 °C with an acidity of 0.336 mmol NH$_3$ g^{-1}. In addition, strong acid sites
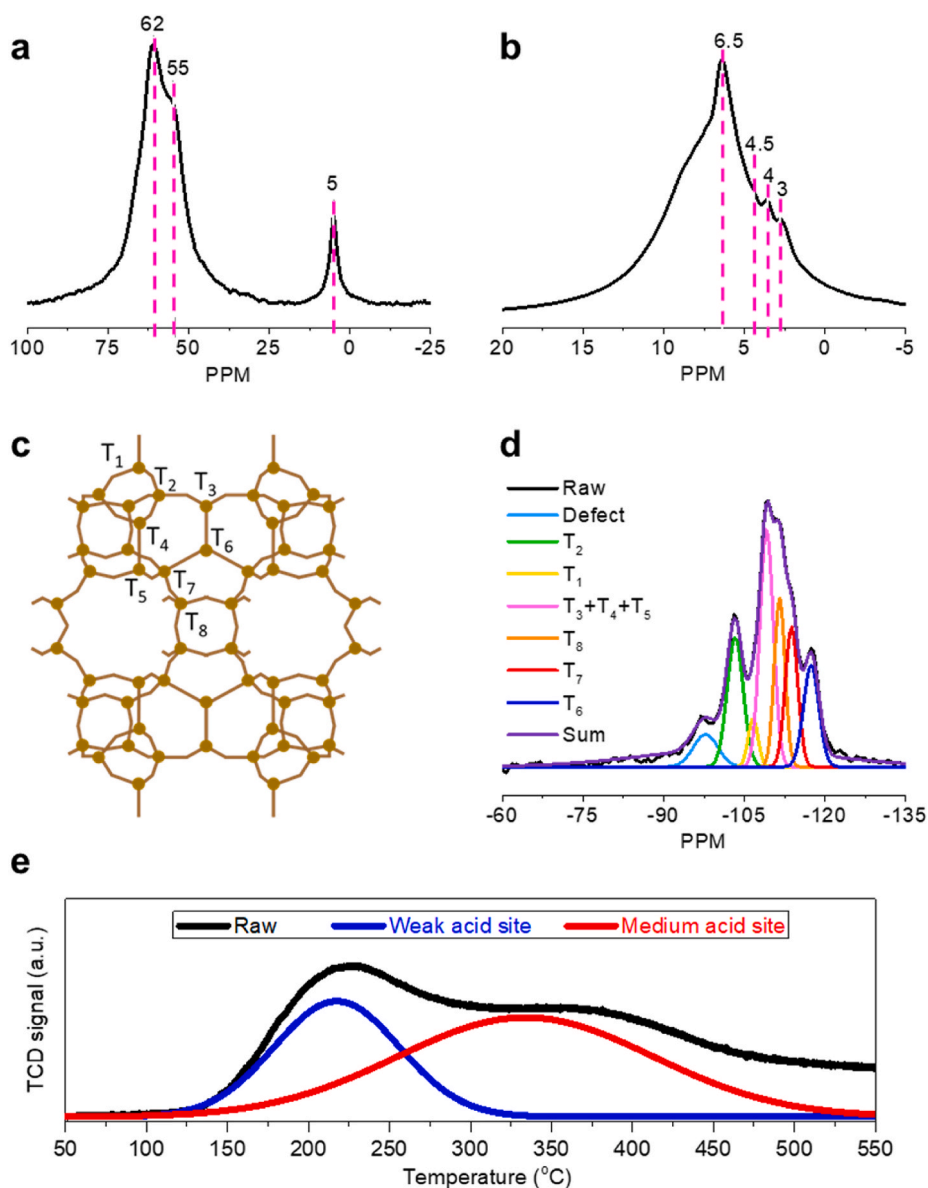
Fig. 7. | Acidity analysis. (a) ^{27}Al and **(b)** ^{1}H MAS-NMR spectra of MCM-22 zeolite synthesized by using RHS and ASG from kaolin at 7 days with the RHS/ASG ratio of 3:1. **(c),** Projection of the MWW-type zeolite unit cell viewed along the b-axis which presents crystallography in a form of a hexagonal structure. **(d),** ^{29}Si MAS-NMR spectra of corresponding MCM-22 zeolite, and **(e),** NH_3-TPD profile of corresponding MCM-22 zeolite.

are absent according to the literature [27] although the total acidity is higher. This investigation clearly verifies that this zeolite sample contains an appropriate number of acidities which associate with Brønsted acid sites.

4. Conclusion

We demonstrated the sustainable solution to synthesis crystalline MCM-22 zeolite with high porosity and large surface area from natural resources including rice husk and natural clay. Kaolin shows more potential for being an Al source than bentonite. Commercial Si sources including TEOS and Na_2SiO_3 show no potential for synthesis of MCM-22 zeolite compared to rice husk silica. A structure formation of zeolite can be developed through a longer reaction time. The surface area and porous properties can be enhanced by the low ratio of RHS/ASG. Moreover, the use of a small RHS/ASG ratio can minimize the defects in zeolite structure with a high amount of Brønsted acid sites. This work opens a new avenue for deriving the catalytic porous materials from natural resources as well as provide fundamental understanding on relationship between synthesis parameters and final product properties which is a key contributing to the environmental materials development.

Author contribution statement

Worapak Tanwongwan: Conceived and designed the experiments; Performed the experiments; Analyzed and interpreted the data; Wrote the paper.

Nuwong Chollacoop: Kajornsak Faungnawakij: Analyzed and interpreted the data.

Suttichai Assabumrungrat: Analyzed and interpreted the data; Contributed reagents, materials, analysis tools or data.

Puritut Nakhanivej: Analyzed and interpreted the data; Wrote the paper.

Apiluck Eiad-ua: Conceived and designed the experiments; Contributed reagents, materials, analysis tools or data; Wrote the paper.

Data availability statement

Data included in article/supp. Material/referenced in article.

Declaration of competing interest

The authors declare that they have no known competing financial interests or personal relationships that could have appeared to influence the work reported in this paper.

Acknowledgement

Appendix A. Supplementary data

Supplementary data to this article can be found online at https://doi.org/10.1016/j.heliyon.2023.e18772.

References

[1] E. Taarning, C.M. Osmundsen, X. Yang, B. Voss, S.I. Andersen, C.H. Christensen, Zeolite-catalyzed biomass conversion to fuels and chemicals, Energy Environ. Sci. 4 (2011) 793–804.

[2] J. Jae, G.A. Tompsett, A.J. Foster, K.D. Hammond, S.M. Auerbach, R.F. Lobo, G.W. Huber, Investigation into the shape selectivity of zeolite catalysts for biomass conversion, J. Catal. 279 (2011) 257–268.

[3] S. Wang, H. Li, S. Xie, S. Liu, L. Xu, Physical and chemical regeneration of zeolitic adsorbents for dye removal in wastewater treatment, Chemosphere 65 (2006) 82–87.

[4] S. Wang, H. Li, L. Xu, Application of zeolite MCM-22 for basic dye removal from wastewater, J. Colloid Interface Sci. 295 (2006) 71–78.

[5] S. Wang, Y. Peng, Natural zeolites as effective adsorbents in water and wastewater treatment, Chem. Eng. J. 156 (2010) 11–24.

[6] Y. Li, L. Li, J. Yu, Applications of zeolites in sustainable chemistry, Chem 3 (2017) 928–949.

[7] R. Zhang, N. Liu, Z. Lei, B. Chen, Selective transformation of various nitrogen-containing exhaust gases toward N2 over zeolite catalysts, Chem. Rev. 116 (2016) 3658–3721.

[8] S. Kumar, R. Srivastava, J. Koh, Utilization of zeolites as CO2 capturing agents: advances and future perspectives, J. CO2 Util. 41 (2020), 101251.

[9] P. Murge, S. Dinda, S. Roy, Zeolite-based sorbent for CO2 capture: preparation and performance evaluation, Langmuir 35 (2019) 14751–14760.

[10] S.-T. Yang, J.-Y. Kim, J. Kim, W.-S. Ahn, CO2 capture over amine-functionalized MCM-22, MCM-36 and ITQ-2, Fuel 97 (2012) 435–442.

[11] N. Yu, R.Z. Wang, L.W. Wang, Sorption thermal storage for solar energy, Prog. Energy Combust. Sci. 39 (2013) 489–514.

[12] J. Ashok, S. Naveen Kumar, A. Venugopal, V. Durga Kumari, M. Subrahmanyam, COX-free H2 production via catalytic decomposition of CH4 over Ni supported on zeolite catalysts, J. Power Sources 164 (2007) 809–814.

[13] Y. Kumagai, A. Kimura, M. Taguchi, M. Watanabe, Hydrogen production by γ-ray irradiation from different types of zeolites in aqueous solution, J. Phys. Chem. C 121 (2017) 18525–18533.

[14] M.K. Rubin, P. Chu, Composition of Synthetic Porous Crystalline Material, its Synthesis and Use, Google Patents, 1990.

[15] M.B. Fernández, J.F. Sánchez M, G.M. Tonetto, D.E. Damiani, Hydrogenation of sunflower oil over different palladium supported catalysts: activity and selectivity, Chem. Eng. J. 155 (2009) 941–949.

[16] M.E. Leonowicz, J.A. Lawton, S.L. Lawton, M.K. Rubin, MCM-22: a molecular sieve with two independent multidimensional channel systems, Science 264 (1994) 1910–1913.

[17] R. Thakkar, R. Bandyopadhyay, Preparation, characterization, and post-synthetic modification of layered MCM-22 zeolite precursor, J. Chem. Sci. 129 (2017) 1671–1676.

[18] P. Sahu, T.V. Haripriya, A. Sreenavya, G.V. Shanbhag, A. Augustin, A. Sakthivel, Alkali/alkaline earth ion-exchanged and palladium dispersed MCM-22 zeolite as a potential catalyst for eugenol isomerization and Heck coupling reactions, J. Chem. Sci. 132 (2020).

[19] P. Sahu, S. Eniyarppu, M. Ahmed, D. Sharma, A. Sakthivel, Cerium ion-exchanged layered MCM-22: preparation, characterization and its application for esterification of fatty acids, J. Porous Mater. 25 (2017) 999–1005.

[20] A. Khaleque, M.M. Alam, M. Hoque, S. Mondal, J.B. Haider, B. Xu, M.A.H. Johir, A.K. Karmakar, J.L. Zhou, M.B. Ahmed, M.A. Moni, Zeolite synthesis from low-cost materials and environmental applications: a review, Environ. Adv. 2 (2020), 100019.

[21] A. Ahmad, S.R. Naqvi, M. Rafique, H. Nasir, A. Sarosh, Synthesis, characterization and catalytic testing of MCM-22 derived catalysts for n-hexane cracking, Sci. Rep. 10 (2020), 21786.

[22] A.J. Schwanke, S. Pergher, Hierarchical MWW Zeolites by Soft and Hard Template Routes, 2018, pp. 1–23.

[23] I. Güray, J. Warzywoda, N. Bac, A. Sacco Jr., Synthesis of zeolite MCM-22 under rotating and static conditions, Microporous Mesoporous Mater. 31 (1999) 241–251.

[24] Y. Cheng, M. Lu, J. Li, X. Su, S. Pan, C. Jiao, M. Feng, Synthesis of MCM-22 zeolite using rice husk as a silica source under varying-temperature conditions, J. Colloid Interface Sci. 369 (2012) 388–394.

[25] E.R.F. dos Santos, A.B. Sousa, R.C.N. Leite, H.M. Laborde, R.R. Menezes, M.G. Freire Rodrigues, Preparation of zeolite MCM-22 using the rice husk ash as silica source, Mater. Sci. Forum 805 (2014) 646–650.

[26] A.S. Kovo, O. Hernandez, S.M. Holmes, Synthesis and characterization of zeolite Y and ZSM-5 from Nigerian Ahoko Kaolin using a novel, lower temperature, metakaolinization technique, J. Mater. Chem. 19 (2009) 6207.

[27] A. Lacarriere, F. Luck, D. Świerczyński, F. Fajula, V. Hulea, Methanol to hydrocarbons over zeolites with MWW topology: effect of zeolite texture and acidity, Appl. Catal. Gen. 402 (2011) 208–217.

[28] J.-G. Li, C.-Y. Tsai, S.-W. Kuo, Fabrication and characterization of inorganic silver and palladium nanostructures within hexagonal cylindrical channels of mesoporous carbon, Polymers 6 (2014) 1794–1809.

[29] M.N. Garaga, M. Persson, N. Yaghini, A. Martinelli, Local coordination and dynamics of a protic ammonium based ionic liquid immobilized in nano-porous silica micro-particles probed by Raman and NMR spectroscopy, Soft Matter 12 (2016) 2583–2592.

[30] Rodrigues, EXPERIMENTAL 2 . 1 Static Synthesis of the MCM-22 (P) Precursor and H-MCM-22 Zeolite, 2010.

[31] V.G. Pol, S.V. Pol, Y. Gofer, J. Calderon-Moreno, A. Gedanken, Thermal decomposition of tetraethylorthosilicate (TEOS) produces silicon coated carbon spheres, J. Mater. Chem. 14 (2004) 966.

[32] J.F. Gomes, A. Sachse, J.R. Gregório, K. Bernardo-Gusmão, A.J. Schwanke, Sustainable synthesis of hierarchical MWW zeolites using silica from an agro-industrial waste, rice husk ash, Cryst. Growth Des. 20 (2019) 178–188.

[33] P. Sahu, A. Tincy, A. Sreenavya, G. Shanbhag, A. Sakthivel, Molybdenum carbonyl grafted on amine-functionalized MCM-22 as potential catalyst for iso-eugenol oxidation, Catal. Lett. 151 (2020) 1336–1349.

[34] X. Gui-Long, D. Changyun, L. Yun, P. Pi-Hui, H. Jian, Y. Zhuoru, Preparation and characterization of Raspberry-like SiO2 particles by the sol-gel method, Nanomater. Nanotechnol. 1 (2011) 21.

[35] F.S.O. Ramos, E.C.O. Munsignatti, H.O. Pastore, 2D–3D structures: the hydrothermal transformation of a layered sodium silicate, Na-RUB-18, into mordenite zeolite, Microporous Mesoporous Mater. 177 (2013) 143–150.

[36] D. Pithadia, V. Hegde, V.P. Brahmkhatri, A. Patel, New catalyst comprising Silicotungstic acid and MCM-22 for degradation of some organic dyes, Environ. Sci. Pollut. Res. Int. 28 (2021) 10633–10641.

[37] J. Vega-Chacón, M. Tarhini, N. Lebaz, N. Jafelicci, N. Zine, A. Errachid, A. Elaissari, Protein-silica hybrid submicron particles: preparation and characterization, Chem. Afr. 3 (2020) 793–801.

[38] H. Zhang, C. Li, J. Guo, L. Zang, J. Luo, In situ synthesis of poly(methyl methacrylate)/SiO2Hybrid nanocomposites via "grafting onto" strategy based on UV irradiation in the presence of iron aqueous solution, J. Nanomater. 2012 (2012) 1–9.

[39] V.A. Ostroumova, A.L. Maksimov, MWW-type zeolites: MCM-22, MCM-36, MCM-49, and MCM-56 (A review), Petrol. Chem. 59 (2019) 788–801.

[40] D. Ma, F. Deng, R. Fu, X. Han, X. Bao, MAS NMR studies on the dealumination of zeolite MCM-22, J. Phys. Chem. B 105 (2001) 1770–1779.

[41] B. Grunberg, T. Emmler, E. Gedat, I. Shenderovich, G.H. Findenegg, H.H. Limbach, G. Buntkowsky, Hydrogen bonding of water confined in mesoporous silica MCM-41 and SBA-15 studied by 1H solid-state NMR, Chemistry 10 (2004) 5689–5696.

[42] M. Hunger, S. Ernst, J. Weitkamp, Multinuclear solid-state nmr investigation of zeolite MCM-22, Zeolites 15 (1995) 188–192.

[43] Y. Li, W. Guo, W. Fan, S. Yuan, J. Li, J. Wang, H. Jiao, T. Tatsumi, A DFT study on the distributions of Al and Brönsted acid sites in zeolite MCM-22, J. Mol. Catal. Chem. 338 (2011) 24–32.